Journal of Alloys and Compounds 536S (2012) S516–S521

Contents lists available at SciVerse ScienceDirect

Journal of Alloys and Compounds

journal homepage: www.elsevier.com/locate/jallcom

Simulation of non-volatile memory cell using chalcogenide glasses

J. Rocca, M. Fontana*, B. Arcondo

Laboratorio de Sólidos Amorfos, INTECIN, Facultad de Ingeniería, Universidad de Buenos Aires – CONICET, Paseo Colón 850, 1063 Buenos Aires, Argentina

ARTICLE INFO

Article history:
Received 24 June 2011
Received in revised form 5 January 2012
Accepted 7 January 2012
Available online 16 January 2012

Keywords:
Numerical simulation
Non-volatile memory
Chalcogenide glasses
GeSbTe system

ABSTRACT

In this paper, a non-volatile memory cell of Te-based chalcogenide material is proposed and modeled. It is formed by layers of three materials: an insulating material, a conductor and a sensitive material: Te-based chalcogenide material. A 2D model using a finite element method has been developed for the simulation of the thermal behaviour of the cell. Temporal evolution of temperature maps is obtained. The model is applied to alloys of the Ge–Sb–Te system. The computed results allow us to understand the role played by the variables involved (thickness of different layers, cell radius, composition of the chalcogenide glass) in order to optimize the cell structure.

1. Introduction

Te-based chalcogenide films are widely used in rewritable compact disks (CD-RW), digital versatile disks (DVD-RW) and are found to be suitable for electrical memories (i.e.: non-volatile memories or phase change memories) [1–5]. A big contrast in their optical and electrical properties is observed when switching between two states: the amorphous and the crystalline phases. In optical applications, information is recorded by the change in optical reflectivity upon the amorphous–crystalline phase transition that is reversibly switched by laser heating [6–9]. While optical disc production is commercialized since late 1980s, reports on phase change memories have grown rapidly in recent years and, interesting and exhaustive reviews of phase change technologies have been published [1,2]. In applications as electrical memories, the material has a high electrical resistivity in the amorphous state, while it has a low resistivity in the crystalline state.

Films with compositions on the $GeTe–Sb_2Te_3$ pseudo-binary system are utilized in these massive memory storage applications. $Ge_2Sb_2Te_5$, $GeSb_2Te_4$ and $GeSb_2Te_7$ are compounds of this pseudo-binary system that have been extensively studied [9–13]. They have the following characteristics: high thermal stability at room temperature, high crystallization rate and very good reversibility between amorphous and crystalline phases [1,2].

A non-volatile memory cell can be switched from a low-resistance crystalline state (SET state) to a high-resistance amorphous state (RESET state), and vice versa. Phase transformation of the chalcogenide film is obtained by Joule heating with the application of a current pulse. In the SET operation, a long low-current pulse is required to reach a temperature between glass and melt temperature. In the RESET operation a short high-current pulse is needed in order to raise chalcogenide film temperature above melting point, thus allowing the transformation into liquid. The liquid state is then quenched in a disordered amorphous phase [1,2,14]. It is intended that the cell current, in particular RESET current, is as small as possible [15].

Several schemes have been proposed and studied using compact models and finite elements simulations with the aim of optimizing the cell structure and making a more efficient memory cell in terms of operation speed, scalability and power consumption [15–24]. Resistor and capacitor networks are used in compact models for knowing the temperature and current [2]. On the other hand, finite elements method shows how the spatial distribution of physical properties influences the electrical current [2]. Two types of cell structures, namely "lance" and "μ-trench" [15,16], have been studied. "Lance" cell models based in 3D finite element method were used in the simulation of thermal performance due to heat generated by applying an electrical pulse [17,18]. Li et al. [18] have shown that the programming current can be reduced by geometric effect. Temperatures in the phase-change layer are calculated using a compact model based on rate equations of crystallization and amorphization [19]. The effect of the Joule heating is investigated in lance cell using finite element method [20]. Multi-physics modeling of phase change memory is used to extract thermal and electrical properties [21]. Temperature distribution in vertical nano-wire phase-change memory cells is also calculated by a compact thermal model [22] or finite element method [23]. The state of the art of physics-based electro-thermal and phase-change model has been reviewed [24].

* Corresponding author.
E-mail address: mfontan2006@gmail.com (M. Fontana).

0925-8388/$ – see front matter © 2012 Elsevier B.V. All rights reserved.
doi:10.1016/j.jallcom.2012.01.052

Several efforts have been dedicated to reduce the current in RESET operation (modifying both geometry and materials) with the aim to achieve more efficient cells. However, some aspects of SET operation (amorphous–crystalline transition) have not been studied yet. The aim of our work is to study the SET operation including in the model the fact that electrical conductivity of the sensitive material is temperature dependent and then analyze the obtained results. Chalcogenide glasses of the Ge–Sb–Te system were used as the sensitive material. Two compositions corresponding to two different zones of the Ge–Sb–Te equilibrium phases diagram were employed: $Ge_2Sb_2Te_5$ and $Ge_{13}Sb_5Te_{82}$. The first zone corresponds to samples with phase change memories properties [14] whereas the second zone's alloys are good glass formers by rapid quenching from the liquid [25]. In particular, the addition of Sb to eutectic alloy $Ge_{15}Te_{85,}$ (e.g. $Ge_{13}Sb_5Te_{82}$) results in a simpler crystallization process at lower temperature [25].

In a previous work, the temperature dependence of the electrical conductivity in $Ge_{13}Sb_5Te_{82}$ thin films was studied [26]. In this work, we want to obtain the memory cell performance for a given geometry and for low currents, focusing on the evolution of temperature in the amorphous–crystalline transition (in the SET operation).

2. Physical description

A 2D scheme of non-volatile memory cell is shown in Fig. 1. It is formed by layers of three materials: an insulating material, a metallic conductor and the sensitive material: chalcogenide glass. Azimuthal symmetry is assumed and therefore, the cylindrical coordinate ρ and z are employed. The sizes of these layers are given by the radial coordinates ρ_1, ρ_2, ρ_3 and ρ_4 and thicknesses L_1, L_2, L_3, L_4 and L_5. We have used chalcogenide materials of the Ge–Sb–Te system. Two compositions corresponding to two different zones of the Ge–Sb–Te equilibrium phases diagram were chosen: (a) $Ge_{13}Sb_5Te_{82}$ (at.%), which is close to eutectic binary $Ge_{15}Te_{85}$, (b) $Ge_2Sb_2Te_5$, which is in the pseudo-binary $GeTe–Sb_2Te_3$ system and has ideal properties for use in non-volatile memory cells, that is, a huge jump in resistivity when the crystal becomes amorphous and vice versa, fast crystallization kinetics and very good reversibility between amorphous and crystalline phases. Alloys with compositions near eutectic binary $Ge_{15}Te_{85}$ show electrical switching that could be used to electronic storage, but the crystallization time is very high for its technological application [14].

The model considers the thermal effect generated by applying an electric pulse on the metallic conductor layers. We assume that the properties (i.e. electrical conductivity) of the cell material are dependent on the temperature. The cell temperature increases due to the heat generated by Joule effect and transferred by conduction inside the cell. Therefore, the temperature spatial distribution is time dependent. On the other hand, the current spatial distribution and consequently the generated heat distribution are dependent on the temperature of each cell point through the conductivity. Therefore, it is an electro-thermal coupled transient problem.We assume that electric and thermal boundary resistances are neglected.

When an electrical potential difference $\Delta V = V_2 - V_1$ is applied on the metallic conductor layers, the electrical potential V inside the cell, can be calculated by solving the Laplace equation [7]:

$$0 = \vec{\nabla}.(\sigma\vec{\nabla}V) \tag{1}$$

with σ the conductivity that is temperature dependent, Eq. (1) has the following boundary conditions:

$$V(\rho,z) = \begin{cases} V_2 & \forall\ \ 0 \le \rho \le \rho_3 \ \text{ and } \ z = z_1 \\ V_1 & \forall\ \ 0 \le \rho \le \rho_3 \ \text{ and } \ z = z_5 \end{cases} \tag{2}$$

with $z_1 = L_1$ and $z_5 = L_1 + L_2 + L_3 + L_4 + L_5$.

The current density $\vec{J}$ can be determined using the Ohm's Law:

$$\vec{J} = -\sigma \cdot \vec{\nabla} V \tag{3}$$

The temperature spatial distribution $T(\rho, z)$ inside the cell and its time dependence are determined by solving the standard heat conduction equation:

$$\delta C_p \frac{\partial T}{\partial t} - \vec{\nabla} \cdot (k\vec{\nabla}T) = Q_v \tag{4}$$

with δ the density, C_p the specific heat, k the thermal conductivity, Q_v the Joule heat per volume unit and per time unit, and t the time. Q_v is calculated using:

$$Q_v = \sigma.\left|\vec{\nabla}V\right|^2 \tag{5}$$

Temperature in Eq. (4) has the following boundary conditions (Similar conditions have been utilized in a previous work [20]):

$$T(\rho,z,t) = \begin{cases} T_0 & z = 0 \ \ \forall \ \ \rho \ \text{ and } \ \forall t \\ T_0 & z = z_5 \ \ \forall \ \ \rho \ \text{ and } \ \forall t \\ T_0 & \rho = \rho_4 \ \ \forall \ \ z \ \text{ and } \ \forall t \end{cases} \tag{6}$$

with T_0, the room temperature.

The initial conditions of Eq. (4) are:

$$T(\rho, z, t = 0) = T_0 \quad \forall \quad \rho \quad \text{and} \quad \forall z \tag{7}$$

3. Numerical analysis – approximation using finite element method

The finite element method (FEM) [27] has been used for the solution of the coupled equations system (1) and (4). The first step is the subdivision of the domain into a set of discrete sub-domains. As mentioned above the problem is 2D, with ρ and z coordinates, therefore we used 2D rectangular element with four nodes (1, 2, 3 and 4) on the corners. A general variable V or T (in our case V is the electrical potential given by Eq. 1, and T is the temperature given by Eq. 4) can be expressed with the node values V_1, V_2, V_3 and V_4 or T_1, T_2, T_3 and T_4, respectively. Thus, the electrical potential and the temperature, for each element, are expressed in the following form:

$$V(u,v) = \sum_{i=1}^{4} h_i(u,v) \cdot V_i = \underline{H} \cdot \underline{V} \tag{8}$$

$$T(u,v) = \sum_{i=1}^{4} h_i(u,v) \cdot T_i = \underline{H} \cdot \underline{T} \tag{9}$$

where $\underline{T} = \begin{bmatrix} T_1 \\ T_2 \\ T_3 \\ T_4 \end{bmatrix}$ is the vector of temperature in the nodes, $\underline{V} = \begin{bmatrix} V_1 \\ V_2 \\ V_3 \\ V_4 \end{bmatrix}$ is the vector of electrical potential in the nodes, $\underline{H} = [h_1(u,v) \ \ h_2(u,v) \ \ h_3(u,v) \ \ h_4(u,v)]$ is the interpolation matrix, where $h_1(u,v) = (1+u)(1+v)/4$, $h_2(u,v) = (1-u)(1+v)/4$, $h_3(u,v) = (1-u)(1-v)/4$ and $h_4(u,v) = (1+u)(1-v)/4$ are called local interpolation functions or shape functions [27] with $-1 \le u, v \le 1$ (u and v are called natural coordinate variables).

In others words, electrical potential or temperature of each element is determined by the values in its nodes using the interpolation functions h_1 h_2 h_3 h_4, that, in this case, are lineal functions of the coordinates.

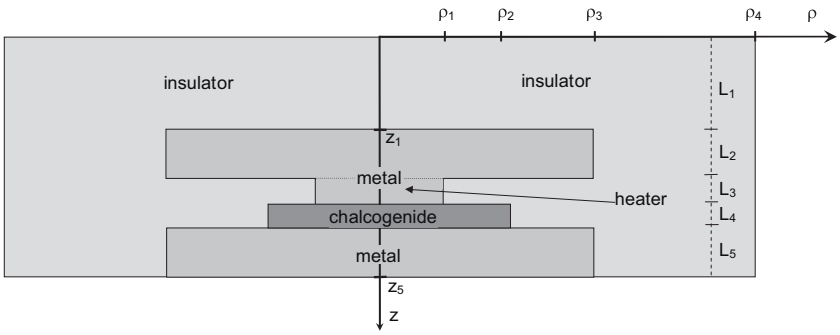

Fig. 1. Structure of the simulated cell.

So, the temporal derivative of the temperature is:

$$\frac{\partial T}{\partial t} = \underline{H}.\frac{\partial \underline{T}}{\partial t} = \underline{H}.\dot{\underline{T}} \tag{10}$$

Using the Galerkin method [27] for Eq. (1):

$$\int_{\Omega} \underline{H}^T.\vec{\nabla}.(\sigma\vec{\nabla}V)d\Omega = 0 \tag{11}$$

With $\underline{H}^T$ the transposed matrix of $\underline{H}$.

Eq. (11) can be written using ρ and z coordinates:

$$\int_{\Omega} \underline{H}^T.\left[\frac{\partial}{\partial\rho}\left(\rho\sigma\frac{\partial(\underline{H}.\underline{V})}{\partial\rho}\right) + \frac{\partial}{\partial z}\left(\rho\sigma\frac{\partial(\underline{H}.\underline{V})}{\partial z}\right)\right]d\Omega = 0 \tag{12}$$

Thus, integrating by parts:

$$\int_{\Omega}\left(\frac{\partial \underline{H}^T}{\partial\rho}\rho\sigma\frac{\partial \underline{H}}{\partial\rho} + \frac{\partial \underline{H}^T}{\partial z}\rho\sigma\frac{\partial \underline{H}}{\partial z}\right)\cdot\underline{V}d\Omega = 0 \tag{13}$$

Therefore, if the electrical conductivity is known, the vector of electrical potential in the nodes of all the elements is obtained using boundary conditions (Eq. (2)) and:

$$\underline{\underline{K_v}}\cdot\underline{V} = 0 \tag{14}$$

With:

$$\underline{\underline{K_v}} = \sum_{\text{elements}}\int_{\Omega}\left(\frac{\partial \underline{H}^T}{\partial\rho}\rho\sigma\frac{\partial \underline{H}}{\partial\rho} + \frac{\partial \underline{H}^T}{\partial z}\rho\sigma\frac{\partial \underline{H}}{\partial z}\right)d\Omega \tag{15}$$

Using Eq. (5), Q_v is:

$$Q_v = \sigma\left|\frac{\partial \underline{H}}{\partial(\rho,z)}\cdot\underline{V}\right|^2 \tag{16}$$

In the same way, using the Galerkin method [27] for Eq. (4):

$$\int_{\Omega}\underline{H}^T.\left(\delta C_p\frac{\partial T}{\partial t} - \vec{\nabla}\cdot(k\vec{\nabla}T) - Q_v\right)d\Omega = 0 \tag{17}$$

Eq. (17) can be written using ρ and z coordinates and Eq. (10):

$$\int_{\Omega}\underline{H}^T.\left[\left(\rho\delta C_p\underline{H}.\frac{\partial \underline{T}}{\partial t} - \left(\frac{\partial}{\partial\rho}\left(k\rho\frac{\partial(\underline{H}.\underline{T})}{\partial\rho}\right)\right.\right.\right.$$
$$\left.\left.\left.+\frac{\partial}{\partial z}\left(k\rho\frac{\partial(\underline{H}.\underline{T})}{\partial z}\right)\right) - \rho Q_v\right)\right]d\Omega = 0 \tag{18}$$

Thus, integrating by parts in the spatial derivates and using Eq. (16):

$$\int_{\Omega}\left[\underline{H}^T\cdot\rho\delta C_p\underline{H}\cdot\dot{\underline{T}} - \left(\frac{\partial \underline{H}^T}{\partial\rho}\cdot k\rho\frac{\partial \underline{H}}{\partial\rho} + \frac{\partial \underline{H}^T}{\partial z}\cdot k\rho\frac{\partial \underline{H}}{\partial z}\right)\right.$$
$$\left.\cdot\underline{T} - \underline{H}^T\cdot\rho\sigma\left|\frac{\partial \underline{H}}{\partial(\rho,z)}\cdot\underline{V}\right|^2\right]d\Omega = 0 \tag{19}$$

Therefore, the vector of the nodes temperatures of all the elements satisfy the following equation:

$$\underline{\underline{C_q}}\cdot\dot{\underline{T}} + \underline{\underline{K_q}}\cdot\underline{T} = \underline{F} \tag{20}$$

With:

$$\underline{\underline{C_q}} = \sum_{\text{elements}}\int_{\Omega}(\underline{H}^T.\rho\delta C_p\underline{H})d\Omega \tag{21}$$

$$\underline{\underline{K_q}} = \sum_{\text{elements}}\int_{\Omega}\left(\frac{\partial \underline{H}^T}{\partial\rho}k\rho\frac{\partial \underline{H}}{\partial\rho} + \frac{\partial \underline{H}^T}{\partial z}k\rho\frac{\partial \underline{H}}{\partial z}\right)d\Omega \tag{22}$$

$$\underline{F} = \sum_{\text{elements}}\int_{\Omega}\left(\underline{H}^T.\rho\sigma\left|\frac{\partial \underline{H}}{\partial(\rho,z)}.\underline{V}\right|^2\right)d\Omega \tag{23}$$

The boundary and initial conditions in Eq. (20) are given by Eqs. (6) and (7). Eqs. (14), (15) and (23) show that the problem is coupled: T is obtained of Eq. (20) if $\underline{F}$ is known, $\underline{F}$ is determined if the electric potential of the nodes $\underline{V}$ and the electric conductivity $\sigma(T)$ are known and for this, temperature must be known.

$\dot{\underline{T}}$ in Eq. (20) can be determined using the α method [27], $\underline{T}$ for the time t is noted $\underline{T}_{(t)}$ and $\dot{\underline{T}}$ for the time $t+\alpha\Delta t$, $\dot{\underline{T}}_{(t+\alpha\Delta t)}$ is written as:

$$\dot{\underline{T}}_{(t+\alpha\Delta t)} = \frac{\underline{T}_{(t+\Delta t)} - \underline{T}_{(t)}}{\Delta T} \tag{24}$$

With $0 \le \alpha \le 1$.

Simulations were done with the condition that cell current was constant with the time. Therefore boundary conditions given by Eq. (2) are changed with the time.

4. Results and discussion

The thermal performance of the non-volatile memory cell is obtained as result of changes in variables involved (cell current, geometry of the different layers and physical properties of the materials – electrical conductivity, thermal conductivity, specific heat, etcetera-). We have found that the results are strongly dependent on following variables: cell current, chalcogenide layer thickness, "heater" radius (see Fig. 1) and electrical conductivity of chalcogenide glass. The geometrical parameters and physical properties of the materials used are shown in Table 1. The temperature dependence of experimental electrical conductivity of the chalcogenide layer was used for each state (amorphous phase and crystal) and for each composition ($Ge_{13}Sb_5Te_{82}$ and $Ge_2Sb_2Te_5$). It presents a big change at the amorphous–crystalline transition temperature.

Fig. 2 shows a 2D diagram that indicates the temperature raised in each part of the memory cell when an electric pulse is applied. The maximum temperature is obtained for the chalcogenide layers in a region near to the "heater". It is in agreement with previous works [1,2,15–18,20,22,24].

Table 1
Geometrical parameters of the cell (see Fig. 1) and physical properties [12,18,26,28] of the materials (with k the thermal conductivity, δ the density, C_p the specific heat, σ the electric conductivity and T_c the crystallization temperature of the amorphous phase) employed in the simulations.

	Metal	Insulator	Chalcogenide alloys	
			Composition 1	Composition 2
Physics data				
Material	TiN	SiO_2	$Ge_{13}Sb_5Te_{82}$	$Ge_2Sb_2Te_5$
k (W/cm K)	0.1 [28]	0.01 [28]	0.002 [28]	0.002 [28]
$\delta \cdot C_p$ (J/cm^3 K)	1.7 [28]	3.1 [28]	1.25 [28]	1.25 [28]
σ (1/Ω cm)	4.5×10^3 [18]	$\approx 10^{-16}$	$2.4 \times 10^6\, e^{-(0.61\,eV/KT)}$ 300 K < T < 404 K	$36.1 \times e^{-(0.243\,eV/KT)}$ T < 423 K
			Amorphous phase	Amorphous phase
			$1.0 \times 10^{25}\, e^{-(2.1\,eV/KT)}$ 404 K < T < 447 K	$1.96 \times 10^5\, e^{-(0.383eV/KT)}$ 423 < T < 633 K
			$7.1 \times 10^9\, e^{-(0.76\,eV/KT)}$ 447 K < T [26]	830 633 < T [12]
			Crystal	Crystal
T_c (K)	–	–	404 [26]	423 [12]

Geometrical data					
Thickness	L_1 (nm)	L_2 (nm)	L_3 (nm)	L_4 (nm)	L_5 (nm)
	1000	150	40	20–150	150
Radius	ρ_1 (nm)	ρ_2 (nm)	ρ_3 (nm)	ρ_4 (nm)	
	10–50	70	200	1200	

Fig. 3 shows a temporal evolution of the maximum temperature inside the cell for different cell currents and for the two Ge–Sb–Te system compositions with the same geometrical parameters. In Fig. 3a, corresponding to $Ge_2Sb_2Te_5$ composition, the simulation with a current of 0.147 μA (associated with a current of 100%) in a pulse of 10 ns is remarked. This value of current is in agreement with previous results [1,24,30] for similar cell geometrical configurations, the current used in our case corresponds to ohmic region in the I–V curve [30]. Raoux et al. [1] points up that current pulses for a fast crystallization of the amorphous structure are in the range 100 ns–1 μs. However, the write time (associated with the amorphous–crystalline transition) in phase change memories is 50 ns [2]. The pulse duration, used in our case, is shorter but is on the order of magnitude. The simulations show that the cell resistance decreases more than an order of magnitude.

Smaller currents (50–90% of 0.147 μA, $Ge_2Sb_2Te_5$ composition, Fig. 3a) are not enough to obtain the crystallization transformation (crystallization temperature = 423 K) whereas it is obtained with higher currents. The crystallization in Fig. 3 is observed with an important jump of the temperature, that is due to abrupt change in the chalcogenide conductivity. In the case of the higher current, a reduction of the temperature is observed after the maximum. This situation, that was not reported previously, can be explained due to the fact that cell resistance decreases with the temperature and

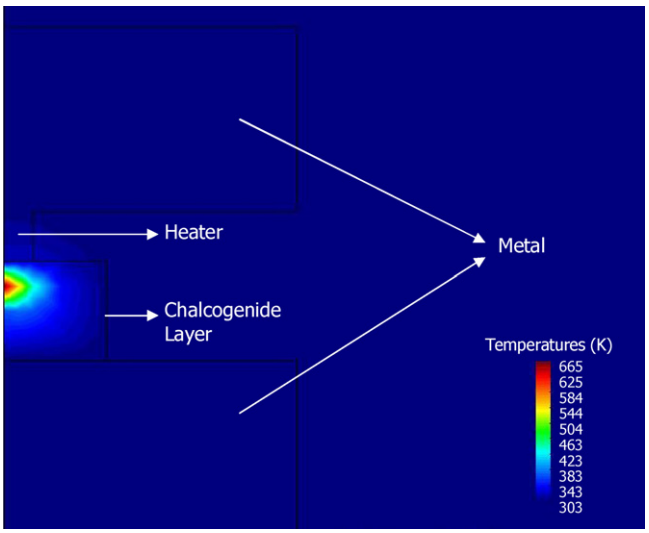

Fig. 2. 2D diagram of the temperature obtained with a pulse of 0.176 μA in 10 ns. The employed geometrical parameters are the chalcogenide layer thickness L_4 = 80 nm and "heater" radius ρ_1 = 20 nm.

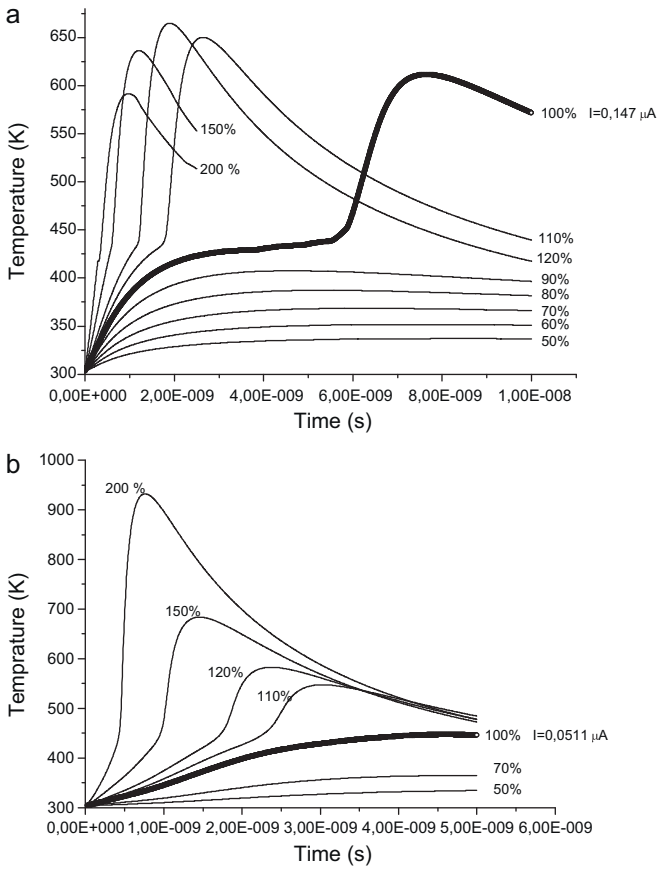

Fig. 3. (a) Temporal evolution of the maximum temperature into the cell for the different cell current (in % of 0.147 μA) with a $Ge_2Sb_2Te_5$ composition. The employed geometrical parameters are the chalcogenide layer thickness L_4 = 80 nm and "heater" radius ρ_1 = 20 nm. (b) Temporal evolution of the maximum temperature into the cell for the different cell current (in % of 0.0511 μA) with a $Ge_{13}Sb_5Te_{82}$ composition. The employed geometrical parameters are the chalcogenide layer thickness L_4 = 80 nm and "heater" radius ρ_1 = 20 nm.

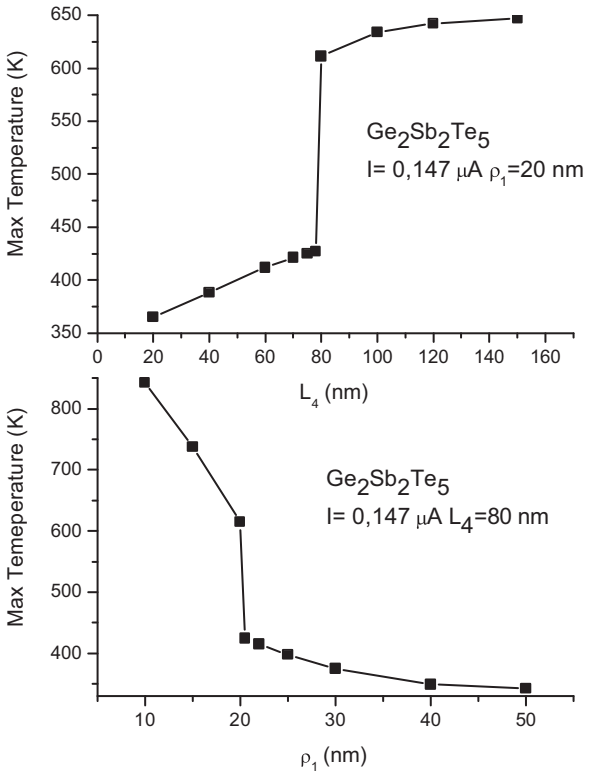

Fig. 4. Maximum temperature into the cell in function of the geometrical parameters: chalcogenide layer thickness L_4 and "heater" radius ρ_1. The employed cell current is 0.147 μA.

therefore the Joule heating effect is not enough to hold the temperature. Similar behaviours are observed in Fig. 3b for $Ge_{13}Sb_5Te_{82}$ composition. In the case of this composition ($Ge_{13}Sb_5Te_{82}$), the electrical potential difference $\Delta V = V_2 - V_1$ applied is about hundreds of Volt (typical 200–400 V), therefore, due to the high voltages, the operation and application of a cell with this composition is more complicated. This difficulty is added to the previously mentioned: alloys $Ge_{13}Sb_5Te_{82}$ are disabled because the crystallization time is very long [14]. On the other hand, $\Delta V = V_2 - V_1$ applied, for the $Ge_2Sb_2Te_5$ composition, is about some Volt (typical 1–30 V). These values of ΔV (hundreds of Volt in $Ge_{13}Sb_5Te_{82}$ composition and some Volt in $Ge_2Sb_2Te_5$ composition) show qualitatively the validity of the simulations.

In Fig. 3a, for the $Ge_2Sb_2Te_5$ composition, the maximum temperature for current of 150% and 200% of 0.147 μA are smaller than current of 120%. This happens because higher currents generate a temperature increment in shorter times and therefore the cell is less time in the zone of higher resistance reducing the Joule effect power.

Fig. 4 shows geometrical dependence of the maximum temperature inside the cell with the same cell current. The employed geometrical parameters are chalcogenide layer thickness (L_4) and "heater" radius (ρ_1). Both figures show an abrupt jump indicating when the crystallization was reached. For the employed current, the cell maximum temperature is higher than the crystallization temperature, both if chalcogenide layer thickness is higher than 80 nm with constant "heater" radius or if "heater" radius is shorter than 20 nm with constant chalcogenide layer thickness.

5. Conclusions

A thermal simulation of a non-volatile memory cell by applying an electric pulse was made. A 2D model using a finite element method has been developed for the simulation of the thermal behaviour of the memory cell. Incubation time for the crystallization [29] is not considered in the model. The temporal evolution of temperature is obtained. The computed results allow us to understand the role played by the variables involved (thickness of different layers, cell radius, composition of the chalcogenide glass).

We have found that the results are strongly dependent on following variables: cell current, chalcogenide layer thickness, "heater" radius and electrical conductivity of chalcogenide glass. For a given geometry and material composition, there is a minimum current to reach temperatures of crystallization of the chalcogenide amorphous inside the cell.

The analysis of the results indicates that alloys with composition $Ge_2Sb_2Te_5$ (in the pseudo-binary $GeTe–Sb_2Te_3$) system present better characteristics than alloys with composition $Ge_{13}Sb_5Te_{82}$.It is interesting to note that due to the sharp jump in electrical conductivity, an abrupt transition in the maximum temperature as a function of cell geometric parameters (chalcogenide layer thickness (L_4) and "heater" radius (ρ_1)) is observed, for a given current and composition of the chalcogenide material.

Acknowledgements

The authors acknowledge support of this work by Agencia Nacional de Promoción Científica y Tecnologica, Consejo Nacional de Investigaciones Científicas y Técnicas and Universidad de Buenos Aires, Argentina.

References

[1] S. Raoux, M. Wuttig (Eds.), Phase Change Materials, Science and Applications, Springer, New York, 2009.
[2] H. Wong, S. Raoux, S. Kim, J. Liang, J. Reifenberg, B. Rajendran, M. Asheghi, K. Goodson, Proc. IEEE 98 12 (2010) 2201.
[3] Z. Sun, J. Zhou, R. Ahuja, Phys. Rev. Lett. 96 (2006), 55507/1–55507/4.
[4] W. Wetnic, M. Wuttig, Nat. Mater. 6 (2008) 20–27.
[5] M. Wuttig, Nat. Mater. 4 (2005) 265–266.
[6] F. Jedema, Nat. Mater. 6 (2007) 90–91.
[7] A. Kolobov, P. Fonds, A. Frenkel, A. Ankudinov, J. Tominaga, T. Uruga, Nat. Mater. 3 (2004) 703–708.
[8] J.A. Kalb, F. Spaepen, M. Wuttig, J. Appl. Phys. 98 (2005), 54910/1–54910/10.
[9] N. Yamada, T. Matsunaga, J. Appl. Phys. 88 (12) (2000) 7020–7028.
[10] N. Yamada, E. Ohno, K. Nishiuchi, N. Akahira, M. Takao, J. Appl. Phys. 69 (5) (1991) 2849–2856.
[11] G. Park, J. Kwon, W. Jo, T. Kim, J. Zuo, Y. Khang, J. Appl. Phys. 102 (2007), 13524/1–13524/5.
[12] I. Friedrich, V. Weidenhof, W. Njoroge, P. Franz, M. Wuttig, J. Appl. Phys. 87 (9) (2000) 4131–4134.
[13] B. Yu, X. Sun, S. Ju, D. Janes, M. Meyyappan, IEEE Trans. Nanotechnol. 7 (4) (2008) 496–502.
[14] M. Wuttig, N. Yamada, Nat. Mater. 6 (2007) 824–832.
[15] U. Russo, D. Ielmini, A. Redaelli, A. Lacaita, IEEE Trans. Electron Dev. 55 (2) (2008) 506.
[16] U. Russo, D. Ielmini, A. Redaelli, A. Lacaita, IEEE Trans. Electron Dev. 55 (2) (2008) 515.
[17] L.P. Shi, T.C. Chong, J.M. Li, D. Koh, R. Zhao, H. Yang, P. Tan, X. Wei, W. Song, Non-Volatile Memory Technology Symposium, 15–17 November, 2004, pp. 83–87.
[18] Y. Li, C. Hwang, T. Li, H. Cheng, Nanotechnology 20 (2009) 285701.
[19] K. Sonoda, A. Sakai, M. Moniwa, K. Ishikawa, O. Tsuchiya, Y. Inoue, IEEE Trans. Electron Dev. 55 (7) (2008) 1672.
[20] G. Beneventi, L. Perniola, Q. Hubert, A. Gliere, L. Larcher, P. Pavan, B. De Salvo, IEEE Trans. Electron Dev. 59 (1) (2012) 188–196.
[21] G. Ferrari, A. Ghetti, D. Ielmini, A. Redaelli, A. Pirovano, Proc. Int. Conf. SISPAD, 2010, pp. 265–268.
[22] I. Chen, IEEE Trans. Electron Dev. 56 (7) (2009) 1523.
[23] W. Chen, J. Guo, J. Appl. Phys. 110 (2011) 84315.
[24] A. Lacaita, D. Ielmini, D. Mantegazza, Solid-State Electron. 52 (2008) 1443–1451.
[25] J.A. Rocca, M. Fontana, B. Arcondo, J. Non-Cryst. Solids 355 (2009) 2068–2073.
[26] J.A. Rocca, M. Fontana, B. Arcondo, M. Molina Ruiz, J. Rodriguez Viejo, Amorphous-crystal transition of Ge-Sb-Te thin films using resistivity

measurements, Humboldt Kolleg - International Conference on Physics (HK2011), March 27-30 (2011) La Plata (Argentina).
[27] K.J. Bathe, Finite Elements Procedure, Prentice Hall, 1996.
[28] A. Redaelli, A. Pirovano, A. Benvenuti, A. Lacaita, J. Appl. Phys. 103 (11) (2008), 111101.
[29] G. Puzzilli, F. Irrera, A. Padovani, P. Pavan, L. Larcher, A. Arya, V. Della Marca, A. Pirovano, Solid-State Device Research Conference, 2008. ESSDERC 2008. 38th European, pp. 158–161.
[30] A. Pirovano, A.L. Lacaita, A. Benvenuti, F. Pellizzer, R. Bez, IEEE Trans. Electron Dev. 51 (3) (2004) 452.